Multi-scale Dynamics of Organic Light-Emitting Devices

A dissertation submitted to the faculty of the graduate school of the University of Minnesota

Kyle William Hershey

In partial fulfillment of the requirements for the degree of Doctor of Philosophy

Russell J. Holmes, Advisor

January 5, 2018

Acknowledgements

I would like to thank my research advisor Russell J. Holmes for all of his guidance and advice.

Parents

Mary Beth

Dow Chemical for funding and collaboration. Dow scientists for research guidance, samples, etc.

Dedication

To some people that I value

Abstract

Over the last decade, organic light-emitting devices (OLEDs) have grown to receive tremendous attention for application in commercial displays and in lighting. While mostly successful for small format displays, challenges still exist that limit their performance for broader applications. Many of these limitations stem from a lack of understanding of charge and exciton dynamics and their impact on efficiency and stability. In this presentation, we describe novel device characterization and modelling efforts aimed at elucidating key dynamic processes in multiple regimes, including the microsecond transient behavior, steady-state, and long term degradation.

A model is presented which unifies both the transient and steady-state electroluminescence behavior of an OLED as a function of current density. The excellent agreement between the model and experiment enables a deeper understanding of efficiency reduction at high brightness. Additionally, the relatively ambiguous device efficiency parameter of charge balance is recast as an exciton formation efficiency. This framework permits a novel characterization paradigm for decoupling degradation pathways during OLED life-testing. In addition to the luminance loss, the degradation in emitter photoluminescence and exciton formation efficiency are also extracted. This technique is applied to an archetypical phosphorescent OLEDs, enabling more comprehensive design rules for device engineering to realize enhanced lifetime. Data science is a rising topic in industrial research. A system for enabling data science techniques within laboratory research is presented. Select useful applications are demonstrated.

Contents

Chapter 1

Overview of Organic Semiconductors

1.1 Organic Semiconductors

1.2 Excitons

1.2.1 Singlets and Triplets

1.2.2 Electronic Transitions

1.3 Charge Transport

Chapter 2

Organic Light-Emtting Devices

2.1 Fabrication Processes

Within our lab, the standard fabrication process for OLEDs is thermal evaporation at base pressures ¡10^{-7} Torr. Substrates consist of glass precoated with indium-tin oxite (ITO). Prior to deposition, substrates are cleaned and treated in a UV-ozone environment. Large area devices on patterned ITO are spin coated with a solution processed hole conducting planarizing layer.

2.2 Characterization

2.2.1 Luminance

2.2.2 Efficiency Analysis

2.3 Historical Developement

2.3.1 The First OLEDs

2.3.2 Phosphorescence

2.3.3 Host-Guest Systems

2.3.4 Cohost Systems

2.3.5 Thermally Activated Delayed Fluorescence

2.4 Device Operation

2.4.1 Dynamic Processes

2.4.2 Efficiency Roll-Off

2.5 Recombination Zone Characterization

2.6 Single Carrier Devices

Chapter 3

Transient and Steady-State Dynamics

This section is an extension of my previous work entitled "*Unified analysis of transient and steady-state electrophosphorescence using exciton and polaron dynamics modeling*".[12]

3.1 Motivation

As discussed in Chapter 2, modern OLEDs are typically based around Phosphorescent emitters in order to realize 100% internal efficiencies.[4, 3, 35, 21] However, these phosphorescent emitters, while allowing emission out of the triplet excitonic state, also suffer from the drawback of a longer exciton lifetime, typically on the order of 10^{-6}-10^{-3} s.[3, 14] An increased lifetime leads to a larger steady-state triplet exciton density compared to a fluorescent device operating at the same luminance. This becomes problematic at the high current densities associated with high brightness due to well documented quenching events.[26, 25, 24, 19, 15, 32, 6] These quenching events lead to a reduced quantum efficiency at high-current, and termed the "Efficiency roll-off".

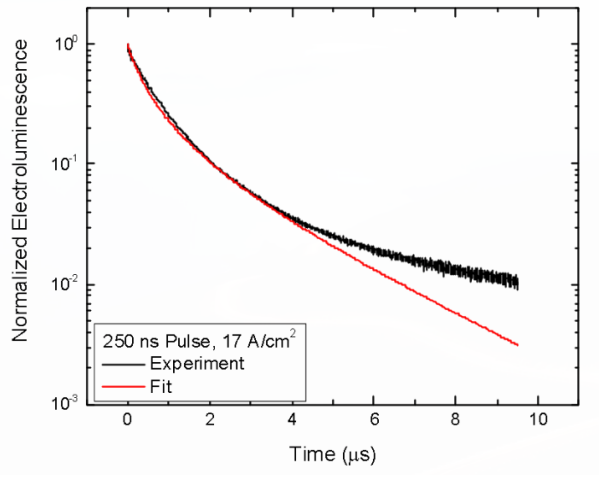

Figure 3.1: Fitting the transient electroluminescence decay without polaron dynamics.

Efficiency roll-off is well attributed to quenching and is ubiquitous to phosphorescent OLED behavior.[26, 6, 20, 8] While previous works have attributed the roll-off to quenching, they have failed to provide a complete picture of the exciton and charge dynamics within the device. All of these works have utilized a

differential equations model for the exciton dynamics, solved in the steady state. This becomes apparent when investigating the transient electroluminescnce (EL), where a transient voltage pulse, on the order of 500 ns is applied to the device and the resulting luminance is recorded as a function of time. Figure 3.1 is an attempt to fit the transient luminance decay using the model presented by Reineke *et al.*[26] which well fits the efficiency roll-off. Indeed, this is a well known problem with existing models, and previous attempts to model the transient EL have utilized an empirical biexponential function to quantifiy the decay.[6, 8, 2, 39] In addition to failing to replicate the luminance decay, no known previous efforts have been made in trying to replicate the experimental transient EL luminance rise.

In addition to the problems with the transient electroluminescence, the interpretation of the existing model without a full dynamics picture can lead to false predictions. Figure 3.2a shows what a quenching model predicts for the roll-off as a function of increasing recombination zone width.[6] However, even in the most idealized case of a gradient emissive layer device, where no additional interfaces come into play, the predictive model fails to replicate the behavior, as shown in Figure 3.2b. While this device is of little interest for further investigation due to the extreme thickness, the point stands that this model has glaring assumptions for it's applications.

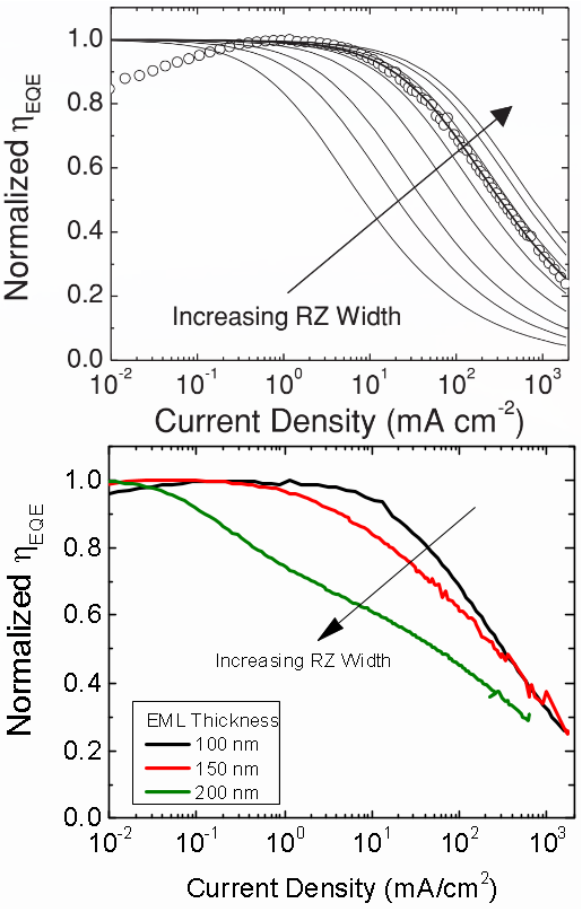

Figure 3.2: (a) Efficiency roll-off predicted by Erickson *et al.* 2014 as a function of recombination zone width.[6] (b) Observed efficiency roll-off for gradient EML devices.

Both the transient EL and the recombination zone dependence issues arise due to an incomplete picture of the device physics, more specifically in the area of polaron dynamics. This work sought to address these issues by including polaron dynamics. Since the steady-state solution of existing models is able to accurately replicate steady-state performance, the transient EL is utilized as well as the steady-state solution to ensure that the underlying physics are accurately captured. A valid solution should be able to accurately fit both regimes using the same model parameter values. In order to leverage previous work, the archetypical green-emitter tris[2-phenylpyridinato-c_2,N]Iridium(III) ($Ir(ppy)_3$) is used for the

extensively characterized photophysics.[4, 2, 34, 1, 16, 17]

3.2 Theory

3.2.1 Exciton Dynamics

The dominannt processes that influence the exciton population, first formalized by Reineke *et al.*[26], have been identified as natural exciton decay, via radiative and non-radiative processes, triplet-triplet annihilation, triplet-polaron quenching, and exciton generation.[6, 32] In triplet-triplet annihilation, two triplets are able to interact, and one exciton transfers its energy to the other, resulting in one molecule relaxing to the ground state and the other forming a hot excited state. This hot state releases this additional energy to heat and typically relaxes back to the T_1 state. Triplet-polaron quenching is the interaction of a polaron with a nearby triplet exciton. Here, one of the charges of the exciton non-radiatively recombines with the polaron of the opposite charge, leaving a remaining loose charge. Excitons are also subject to field dissociation, but this mechanism is ignored in this work. Field dissociation is typically observed for fields larger than 2.5×10^6 V/cm. This is near the maximum field used for this study, and would be important to consider for higher voltage characterization.

In agreement with previous models, singlet-triplet exciton intersystem crossing and host-guest exciton energy transfer are assumed to be fast compared to exciton decay.[26, 2, 36] Since these mechanisms are much faster, they will not be rate-limiting processes and can thus be omitted from the differential equations model without sacrificing accuracy. Within an operational device, electron and hole populations are indistinguishable. Therefore, the electron (n_e) and hole (n_h) densities are treated as a single geralized polaron population, $n_{pol} = n_e + n_h$. For simplicity, the model developed here treats the exciton and polaron populations as spatially uniform and confined to the exciton recombination zone. An spatial inhomogeneity in exciton and polaron density as well as their overlap is absorbed into the bimolecular rate constants. It is important to note that due to this assumption, rate constants are a property of the device stack, and not just a material property. With these assumptions, the dynamic processes determining exciton density (n_{ex}) can be summarized in the following one-dimensional rate equation:

$$\frac{dn_{ex}}{dt} = -\frac{n_{ex}}{\tau} - \frac{1}{2}k_{\text{TT}}n_{ex}^2 - k_{\text{TP}}n_{pol}n_{ex} + G_{ex} \tag{3.1}$$

where τ is the natural exciton lifetime, determined by the radiative (k_r) and non-radiative (k_{nr}) decay rates by $\tau = 1/(k_r + k_{nr})$, $k_{\text{TT}}$is the rate constant for triplet-triplet annihilation, $k_{\text{TP}}$is the rate constant for triplet-polaron quenching, and G_{ex} is the exciton generation rate. As this is a one-dimensional model, G_{ex}

is a spatially uniform generation rate, a simplifying assumption. Many studies have modeled the exciton recombination zone profile, relying on material energy levels, as well as mobilities.[27, 9, 10, 29, 30] While these models are more accurate and explicit, in the way that they capture the physics, they also increase the dimensionality of our model, as well as increasing the parameterization; requiring seperate electron and hole rate equations, mobilities and energy levels for every material. Even with this increased accuracy of the physical processes, identifying if the predicted exciton recombination zone is accurate requires significant additional measurements. Since the goal of this work is to provide a functional model to accurately predict the transient and steady-state device behavior, spatially uniform dynamics are assumed. Here, exciton formation is treated using a Langevin recombination formalism based on the polaron density.[29, 22, 5]

$$G_{ex} = \frac{k_{\text{F}}}{4} n_{pol}^2 \tag{3.2}$$

where $k_{\text{F}}$is the rate constant for exciton formation. The factor of four accounts for the diversity of the polaron population and assumes that electrons and holes are in equal proportion. The accuracy of this prefactor is reduced for imbalanced charge, and is investigated in Section 3.7.2. For n_e:n_h ratios 2:1 or better, less than 20% error is found in this term.

3.3 Polaron Dynamics

Previous models for efficiency roll-off have ignored polaron dynamics and assumed that all polarons readily form excitons. The steady-state polaron density is then modeled using a space charge limited model.[23] To attribute physics to this process, a simple picture of polaron dynamics is assumed, consisting of charge injection and transport, exciton formation, and polaron loss. In order to preserve our one-dimensionality, polarons must be uniformly distributed. Without competing losses in the tranport layers, all injected polarons must eventually reach the emissive layer. We further assume that polarons easily enter that emissive layer and that the majority of polaron build up occurs within the emissive layer, rather than the transport layers. Therefore, the charges injected from the current density, J, are uniformly generated in the emissive layer by $G_{pol} = 2J/ew$. Here, e is the electron charge, and the factor of two arises from an assumption of equal charge injection. In a well balanced device, the measured current forms holes on one side of the device and electrons on the other, and are both injected into the device. This is discussed extensively in Section 3.7.1 Polaron losses to exciton formation mirror the exciton formation rate presented in Equation 3.2, though at twice the rate due to two polarons forming one exciton.

The introduction of polaron loss from the emissive layer through the device without forming excitons is

essential to address the limitations of previous models. Without this term, peak internal quantum efficiency of all devices is assumed to be 100% and and the roll-up of efficiency at low current can not be explained. In order to capture polaron loss, a first order approximation is made for loss in that only the majority charge carrier can be lost and leaks through the device with a characteristic time, τ_l. With these mechanisms, the full polaron dynamics can be expressed as:

$$\frac{dn_{pol}}{dt} = \frac{-k_{\mathrm{F}}}{2} n_{pol}^2 - \frac{n_{pol}}{\tau_l} + G_{pol}. \tag{3.3}$$

3.3.1 Transient Electroluminescence

In this work, given a full model for polaron dynamics, the model is easiest to solve starting from the application of the current pulse, rather than at peak luminace. Under pulsed electrical excitation, Equations 3.1 and 3.3 can be solved at the beginning of the pulse with the initial conditions $n_{ex} = n_{pol} = 0$. Upon the application of a voltage pulse, there is a time delay before polarons reach the emissive layer, as evidenced by the delay in luminance turn on. This has been previously attributed to charge injection and transport in the emissive layer.[37] The injection time varies with device area due to the device capacitance and accounts for the majority of the delay time for large devices. Transport is dependent on the mobility, as well as the field, which is a function of time due to the device capacitance. These times can be well predicted using the following equations:

$$t_{inj} = \tau \log(1 - \frac{V_{th}}{V_0} \tag{3.4}$$

$$d = \int_0^{t_{trans}} \mu_0 E_0 \exp\left(\sqrt{\gamma E_0 \left[1 - \left(1 - \frac{V_{th}}{V_0}\right) e^{-t/\tau}\right]}\right) \left[1 - \left(1 - \frac{V_{th}}{V_0}\right) e^{-t/\tau}\right] dt \tag{3.5}$$

where τ is the RC time constant of the device, V_{th} is the voltage injection threshold, t_{inj} is the injection time, t_{trans} is the transport time, d is the tranport layer thickness, μ_0 is the base mobility, γ is the field dependent mobility term, E_0 is the field and V_0 is the voltage. A prediction of the delay time as well as experimental values are shown in Figure **??**. Interestingly, the functional dependence of the model accurately reproduces the extracted data. The mismatch in absolute value is due to the use of the geometric capacitance in the model.

After this delay, constant current polaron generation is assumed for the remainder of the voltage pulse to calculate polaron generation. When the voltage pulse is removed, G_{pol} goes to 0 and the decay can be solved using Equations 3.1 and 3.3. This model does allow polarons to continue to form excitons after the

voltage has been removed. In the transient regime, if the pulse width is shorter than τ_l, polarons are not able to traverse the emissive layer during the voltage pulse. Once the voltage is removed, there is no longer a driving force for polaron leakage via drift. Under this assumption, the leakage term in Equation 3.3 can be ignored. After the full device behavior is fit, the validity of this assumption can be assessed based on the fit values for τ_l.

3.3.2 Efficiency Analysis

The maximum external quantum efficiency of an OLED is often expressed as[3, 28]

$$\eta_{\mathrm{EQE}} = \eta_{\mathrm{OC}}\eta_{\mathrm{PL}}\chi\eta_{\mathrm{EF}} \tag{3.6}$$

where $\eta_{\mathrm{EQE}}$is the external quantum efficiency, $\eta_{\mathrm{OC}}$is the out-coupling efficiency, $\eta_{\mathrm{PL}}$is the photoluminescence efficiency of the emissive molecule, *chi* is the fraction of excitons that are quantum mechanically allowed to emit (In the case of phosphorescent molecules, $\chi = 1$ and γ is typically referred to as the charge balance. While frequently applied, this expression suffers from two major limitations. First, there is no accounting for losses due to exciton quenching, and second, charge balance losses are not strictly defined. Since this equation is intended for the maximum efficiency, further modification would have to be done to account for quenching, as is done in Chapter 4. The charge balance factor, γ is typically used as a correction factor to account for differences between the observed $\eta_{\mathrm{EQE}}$and the other calculated factors in Equation 3.6. It is widely hinted at that charge balance relates to the carrier balance, but no formalism is ever given, so it cannot be calculated. Given our full dynamics model, we are able to be explicit in both of these areas in a meaningful way. The internal quantum efficiency of a device is simply the ratio of the radiative exciton rate to the rate of electron injection, and we can therefore recast Equation 3.6 as

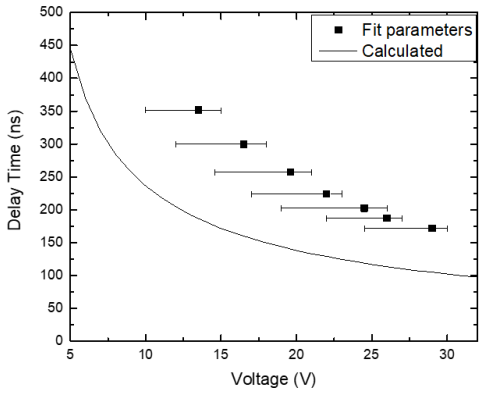

Figure 3.3: Extracted polaron injection time is shown as a function of voltage along with a fit from the model.

$$\eta_{\mathrm{EQE}} = \eta_{\mathrm{OC}}\frac{n_{ex}k_r}{G_{pol}/2}. \tag{3.7}$$

Note that in this equation, exciton quenching is accounted for in the n_{ex} term because in the steady-state, n_{ex} is reduced according to this quenching, which is competative with k_r. Dynamically, the charge balance factor is the fraction of injected polarons contributing in exciton formation. This can be viewed as

the efficiency of Equation 3.3 to form excitons. Given this interpretation, we will recast the charge balance factor γ, as an explicitely defined exciton formation efficiency η_{EF}as

$$\eta_{\mathrm{EF}} = \gamma = \frac{\frac{1}{2}k_{\mathrm{F}}n_{pol}}{G_{pol}} = \frac{\frac{1}{2}k_{\mathrm{F}}n_{pol}}{\frac{1}{2}k_{\mathrm{F}}n_{pol} + \frac{1}{\tau_l}} \tag{3.8}$$

Equations 3.7 and 3.2 allow us to rigorously tie $\eta_{\mathrm{EQE}}$and $\eta_{\mathrm{EF}}$to dynamic processes within the device in a quantitative manner.

3.4 Experimental Details

Devices used for measurements of transient and steady-state EL had the following structure: ITO (150 nm)/poly(3,4-ethylenedioxythiophene)-poly(styr- enesulfonate) (PEDOT-PSS) (40 nm)/tris(4-carbazoyl-9-ylphenyl)amine (TCTA) (30 nm)/10% tris[2-phenylpyridi- nato-C2,N]Iridium(III) ($Ir(ppy)_3$) doped in 4,40-Bis(N- carbazolyl)1,10-biphenyl (CBP) (10 nm)/bathophenanthro- line (Bphen) (30 nm)/LiF (1 nm)/Al (100 nm). Transient PL decays were measured using 60-nm-thick films of CBP doped with 10% $Ir(ppy)_3$deposited on quartz slides. The hole-only device structure used for steady-state PL quenching measure- ments had the following structure: ITO (150 nm)/PEDOT-PSS (40 nm)/10% $Ir(ppy)_3$in CBP (60 nm)/Au (50 nm). The gold cathode was used to prevent electron injection. Transient EL measurements were conducted using a voltage pulse generator (HP 8114a) with pulse amplitudes ranging from 540V and pulse widths ranging from 250 ns500 ns with a period 500 ls. Luminescence was recorded using a set of collection lenses focused onto a fast photodiode (Thorlabs DET36A). The photodiode signal was recorded using an oscilloscope (Tektronix TDS5104b). Transient PL measurements were collected using a pulsed nitrogen laser (Optical Building Blocks) with a pulse length of approximately 1 ns and emission wavelength of λ= 337 nm at a repetition rate of 6 Hz. Laser light was focused on the sample using a series of lenses, with collec- tion carried out using the same techniques already described for transient EL. Incident laser power was measured using a Coherent EnergyMax 10MB-HE detector. Film thicknesses and optical constants used for modeling the out-coupling efficiency in Eq. (9) were obtained using a J. A. Woollam variable angle spectroscopic elllips- ometer (VASE) using a Cauchy dispersion model.

3.5 Exciton Quenching in Photoluminescence

Photoluminescence measurements have been previously used to extract the rate constants for triplet-triplet annihilation and triplet-polaron quenching.[6, 26] This is important because it allows an independent confirmation of the extracted rate constants extracted during the electroluminescence fitting. The transient

photoluminescence exposes the natural exciton lifetime, τ and at high incident flux, the triplet-triplet annihilation rate constant, k_{TT}. This measurement involves an incident laser pulse, in this case, from a 337 nm nitrogen laser, which is able to excite a large exciton population. The pulse width of the nitrogen laser is 1ns and is much faster than τ or k_{TT}, allowing us to use Equation 3.1 with the initial boundary condition $n_{ex} = A(E_{\text{pulse}}/hfV)$ where A is the absorbed fraction of photons, E_{pulse} is the pulse energy, hf is the photon energy and V is the film volume. Since this is optical only excitation, the other boundary condition is $n_{pol} = 0$ and we can ignote Equation 3.3.[26, 6, 2] For CBP films doped with Ir(ppy)_3, good agreement with the model is observed across a range on initial exciton densities, as shown in Figure 3.4(a). The exciton lifetime, τ was found to be mostly independent of exciton density and was globally fit to 1.5±0.2 μs. The triplet-triplet annihilation rate constant appears to be a function of intensity and ranges from $k_{\text{TT}} = 2.4 \times 10^{-13}$ cm^3/s at $n_{ex_0} = 4.1 \times 10^{18}$ cm^{-3} to $k_{\text{TT}} = 6.9 \times 10^{-14}$ cm^3/s at $n_{ex_0} = 1.1 \times 10^{20}$ cm^{-3}. These extracted values and trend with intensity are in good agreement with previous reports.[26, 6, 33] It is important to note, that the exciton environment is very important for these values. Previous studies have shown that the presence of a metal cathode on top of thhe film can significantly reduce the exciton lifetime by allowing additional non-radiative recombination via surface plasmon coupling.[31] This becomes important in the comparison of these parameters with those obtained under electroluminescence within a device. A more representative experiment would have involved a full device stack with cathode, rather than just a film. Alas, I did not have that forsight for this experiment.

Triplet-polaron quenching rate constant measurement is done in single carrier devices as a function of polaron density. It is largely uninvestigated as to the differences between electrons and holes, but in previous works, hole only currents are used, a precident which will be followed in this work.[6, 26] A steady-state exciton population is generated optically, in this case, a 405 nm laser. In a single carrier device, a space charge limited current model featuring an exponential trap distribution is often used.[18, 7, 23] This model is employed largely because it fits the obtained current-voltage behavior most closely. In reality, a single trap state would be expected, as that is what is introduced by Ir(ppy)_3in a doped film. These models are frequently employed, despite their inaccuracies, largely for simplicity. A more accurate determination of polaron density is discussed in Chapter **??**. However, in a space charge limited model with an exponential trap distribution, the current density voltage relationship can be modeled using

$$V = \left[\frac{J}{e\mu N_C} d^{2l+} \left(\frac{eN_0 k_B T_t}{\epsilon}\right)^l\right]^{\frac{1}{l+1}} = CJ^{\frac{1}{l+1}}, \tag{3.9}$$

where N_C is the density of states at the transport level, ϵ is the permittivity, μ is the mobility, L is the device thickness and $l = T_t/T$ with T_t being an experimentally determined characteristic temperature of the

trap distribution. The Polarond density is then given by

$$n_{pol} = eN_c \left(\frac{\epsilon V}{ed^2 N_0 k T_t} \right)^l . \tag{3.10}$$

Combining Equation 3.10 with Equation 3.1, the ratio of the steady-state PL intensity (L) to the PL intensity in the absence of polarons (L_0) can be written as[26]

$$\frac{L(n_{pol}}{L_0} = \frac{1}{1 + \tau k_{\text{TP}} n_{pol}} \tag{3.11}$$

After fitting the current density-voltage characteristics of the device are fit using Equation 3.9, Equations 3.10 and 3.11 can be used to extract the triplet-polaron rate constant for a given value of τ. In this case, we use τ as extracted from the transient PL measurements. The fit obtained for a CBP Ir(ppy)$_3$hole only device is shown in Figure 3.4b. This devices utilizes a gold cathode to prevent electron injection and shows minimal exciton formation, as expected. The organic stack is the same as the emissive layer of the inviestigated device. In fitting the current density-voltage characteristics using Equation 3.9, a value of $l = (2.4 \pm 0.2)$ was found. The extracted triplet-polaron quenching rate constant from fitting Equation 3.11 was $k_{\text{TP}} = (2.8 \pm 0.2) \times 10^{-13}$ cm^3/s and is agreement with previous measurements.[6, 26]

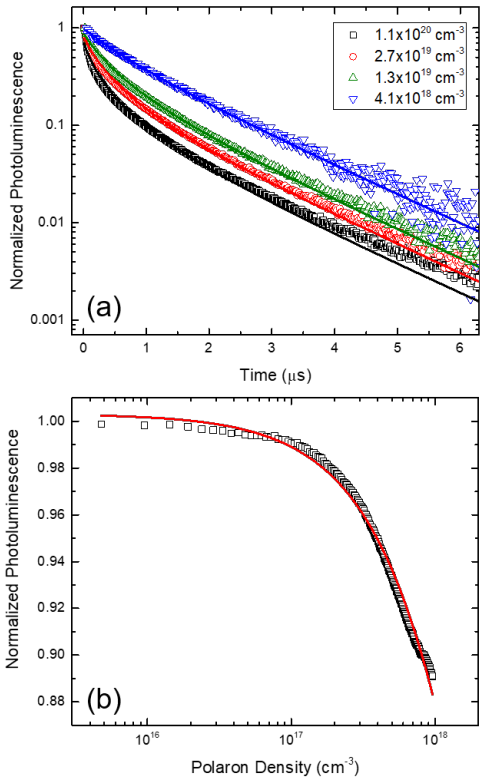

Figure 3.4: (a) Transient photoluminescence (PL) decays for several initial exciton densities with fits shown as solid lines using Eqn. 3.2. Fit parameters are discussed in SECTION. Exciton densities are calculated using measured incident power and beam size in combination iwht Beer's Law. (b) Steady-state PL quenching as a function of polaron density and the resulting fit from Eqn. 3.11 shown as the solid line.

3.6 Application to Devices

In order to fit both the steady-state and transient regimes, decisions need to be made as to a methodology for extracting parameters. The obvious choice

may seem to be to try to produce a global fit by fitting both regimes simultaniously. The major draw back of this approach is the value of τ_l. Since this is a function of the applied field, this is not single valued and relies on knowing the field dependence. Additionally, the steady-state provides little insight into the actual quantities of τ, k_{TT}, k_{TP}, and k_{F}, and only the ratio of radiative and non-radiative processes is needed for a quality fit of the efficiency roll-off. Additionally, within this model, only n_{ex} is experimentally available to fit, and the fit parameters are not independent. The most obvious example of this is the values of $k_{\text{TT}}$and k_{TP}, which have similar impact on the exciton population and similar formulation. This makes it near impossible to distinguish a dominant mechanism between these two, and results for exact values of quenching constants need to be considered with caution. This methodology only gives a net effect of the two quenching mechanisms in total, rather than a true seperate measurement of both quantities as is obtained in the PL quenching measurements, discussed in Section 3.5.

With these limitations addressed, the method used for this discussion to fit all of the device physics has been carefully considered to achieve the highest parameter sensitivity. The bimolecular quenching constants are most sensitive to the efficiency roll-off since small changes in the quenching constants make a large impact on the roll-off behavior. However, the lifetime and exciton formation can only be determined to within a fixed ratio. In contrast, the exact values of lifetime and exciton formation rate are critical to the behavior of the transient EL while the bimolecular quenching constants are dif-

ficult to probe in the current regime investigated. In order to use these sensitivities, a quenching only model (ignoring τ_l) to fit the normalized efficiency roll-off, such has been previously reported, is used to determine the bimolecular quenching rates, k_{TT} and k_{TP}. Quenching only models can only fit the normalized η_{EQE} roll-off because without a polaron loss term, η_{EF} is assumed to be 100% and the exact magnitude of efficiency cannot be reproduced. Initial values for all parameters, except k_F which is previously unmeasured, are determined by the photoluminescence measurement values. With these quenching rates fixed, the transient EL is fit using Equations 3.1 and 3.3 in order to determine τ and k_F. Remember that in the transient regime for short pulses, we can assume that $\tau_l = \infty$ and can be ignored.

With these critical rate constants determined, we will revisit the efficiency as a function of current density. In the first pass, we ignored the exact value of efficiency and only fit the normalized roll-off. Now, since we know the other parameters, we can revisit η_{EQE}, now matching the exact profile for all currents, by conducting a point-by-point fit for k_F. This fit for k_F can then be used to calculate η_{EF} and can be compared to a drift model, to assess its validity.

3.6.1 Initializing Parameters with Quenching Only Steady-State Model

3.6.2 Transient Modeling

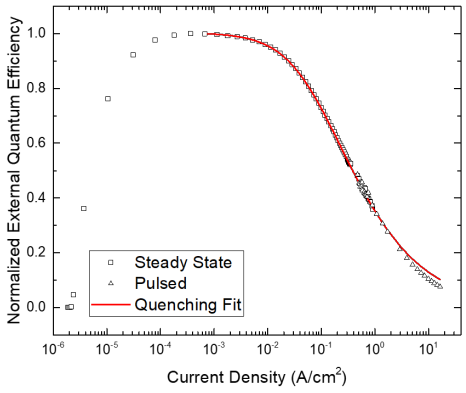

Figure 3.5: Normalized experimental η_{EQE} as a function of current density. Solid line is a fit to the data using Eqn. 3.1 and 3.3 in the absence of polaron loss. Pulsed eqe measurements are conducted using low duty cycle pulses to steady-state luminance to reduce Joule heating in device.

	Transient EL	Efficiency Roll-off
τ (s)	$6.9 \pm 0.1 \times 10^{-7}$	6.1×10^{-7}
$k_{\mathrm{TT}}(\mathrm{cm}^3/\mathrm{s})$	7.1×10^{-12}	7.1×10^{-12}
$k_{\mathrm{TP}}(\mathrm{cm}^3/\mathrm{s})$	3.3×10^{-13}	3.3×10^{-13}
$k_{\mathrm{F}}(\mathrm{cm}^3/\mathrm{s})$	$7.7 \pm 3.5 \times 10^{-12}$	1.6×10^{-11}

Table 3.1: Fit parameters extracted from transient and steady-state electroluminescence. Transient EL fit parameters averaged over all measured current densities. η_{EQE} roll-off parameters averaged over several measured devices. Triplet-triplet annihilation and triplet-polaron quenching rates are fixed to those obtained from fitting the normalized efficiency roll-off.

3.6.3 Term Efficiency During Transient

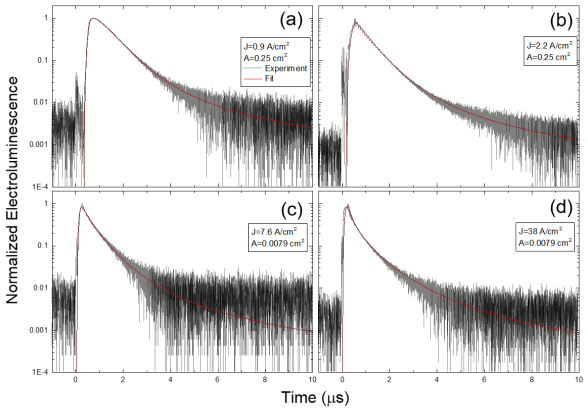

Figure 3.6: Transient electroluminescence (EL) for four different current densities (J) and device areas (A). (a) 0.25 cm^2 device at a current density during the pulse of J = 0.9 A/cm^2 (b) 0.25 cm2 device at J = 2.2 A/cm^2 (c) 0.0079 cm^2 device at J = 7.6 A/cm^2 (d) 0.0079 cm^2 device at J = 38 A/cm^2

3.6.4 Extracting Exciton Formation Efficiency

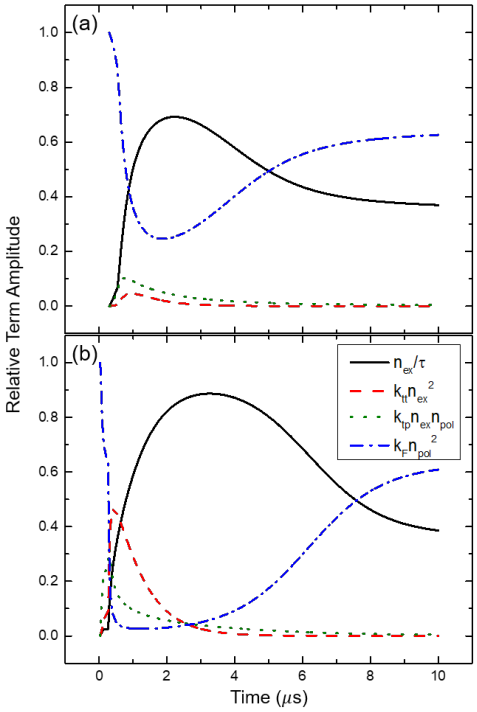

Figure 3.7: Term efficiency for each dynamical process influencing the exciton population for (a) 0.25 cm^2 device operated at 0.9 A/cm^2 for 500 ns and (b) 0.785 mm^2 device operated at a current density of 38 A/cm^2 for 250 ns. Relative term amplitude is calculated as the magnitude of each term in Eqn. 3.1 divided by the sum of absolute values of each term.

3.6.5 Drift Model

$$\tau_l = \frac{w}{E\mu(E)} \tag{3.12}$$

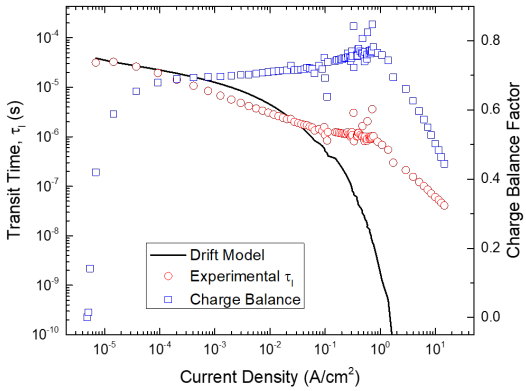

Figure 3.8: Transit time extracted from η_{EQE} measurements are shown as the red circles. Predictions using the drift model are calculated using Eqn. 3.12. The drift model assumes a uniform electric field. Good agreement between the experimental transit time and the drift model is found for a field distributed over 20 nm. The charge balance factor is shown as a function of current density in blue squares.

3.7 Understanding Assumptions of Polaron Model

3.7.1 Carrier Injection

$$\frac{dn_h}{dt} = -k_{\mathrm{F}} n_e n_h - \frac{n_h}{\tau_{lh}} + \frac{J_h}{ew} \tag{3.13}$$

$$\frac{dn_e}{dt} = -k_{\mathrm{F}} n_e n_h - \frac{n_e}{\tau_{le}} + \frac{J_e}{ew} \tag{3.14}$$

$$J_1 \rightarrow J_h = J_2 \rightarrow J_e \tag{3.15}$$

$$\frac{J_e}{ew} + \frac{J_h}{ew} = \frac{J_1 + J_2}{ew} = \frac{2J}{ew} \tag{3.16}$$

$$J_1 = J_h \tag{3.17}$$

$$J_2 = J_e + J_l \tag{3.18}$$

$$J = J_h = J_e + J_l \tag{3.19}$$

$$G_{pol} - \frac{J_l}{ew} = \frac{2J - J_l}{ew} \tag{3.20}$$

3.7.2 Charge Imbalance

$$\alpha = \frac{n_h}{n_e + n_h} \tag{3.21}$$

$$\left[\frac{dn_{pol}}{dt}\right]_{formation} = -2k_{\mathrm{F}} n_{pol}^2 \alpha(1-\alpha) \tag{3.22}$$

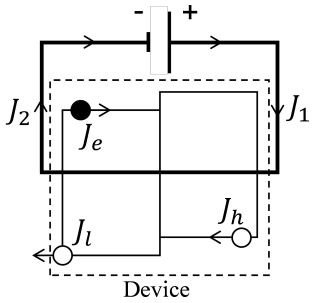

Figure 3.9: Current density formalism within the circuit. and are the currents measured on either side of the device. and are the electron and hole currents within the device and is the unbalanced current, assumed to be only holes, that leaks out of the opposing contact.

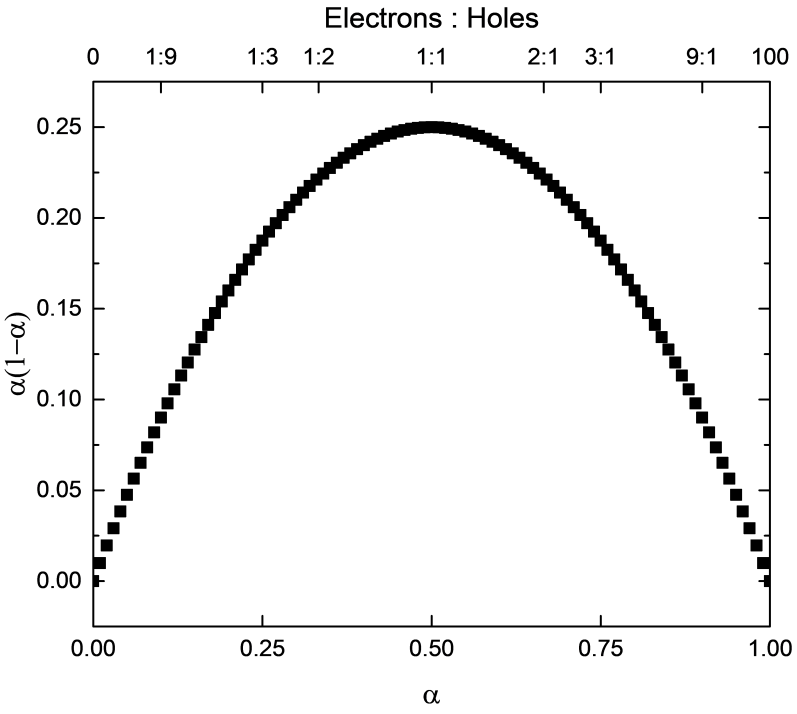

Figure 3.10: The quantity $\alpha(1-\alpha)$ is plotted as a function of the polaron composition, α and the electron to hole ratio.

Chapter 4

Integrated Photoluminescence Lifetimes

4.1 Luminance as Efficiency Loss

$$\eta_{EQE} = \eta_{PL}\eta_{OC}\chi\eta_{EF}\eta_{\tau} \tag{4.1}$$

$$\frac{\eta_{EQE}(t)}{\eta^0_{EQE}} = \frac{\eta_{PL}(t)}{\eta^0_{PL}}\frac{\eta_{EF}(t)}{\eta^0_{EF}} \tag{4.2}$$

4.2 Photoluminescence Characterization

$$\frac{\eta_{PL}(t)}{\eta^0_{PL}} = \frac{L_{PL}(t)}{L^0_{PL}}\frac{I^0}{I(t)} \tag{4.3}$$

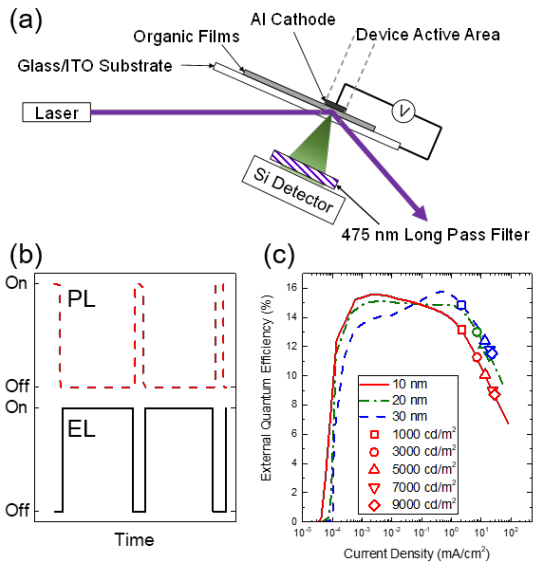

Figure 4.1: (a) Experimental configuration for the measurement of electro- (EL) and photoluminescence (PL) during OLED degradation. Laser excitation is incident on a subsection of the device area. The laser is aligned so that neither the incident nor reflected beam strikes the detector. Stray laser light is removed by a λ=475 nm dielectric long pass filter. (b) Excitation scheme. EL and PL signals are probed independently with no temporal overlap. (c) External quantum efficiency versus current density and luminance for devices having emissive layer thickness of 10 nm, 20 nm and 30 nm.

4.2.1 Light Selection

4.2.2 Absorption - Recombination Overlap

4.2.3 Contact Degradation

4.2.4 Quenching Changes During Degradation

4.2.5 Verification with Excton Lifetime

4.3 Experimental Implementation

4.3.1 Hardware Setup

4.3.2 Software Developement

4.3.3 Database Integration

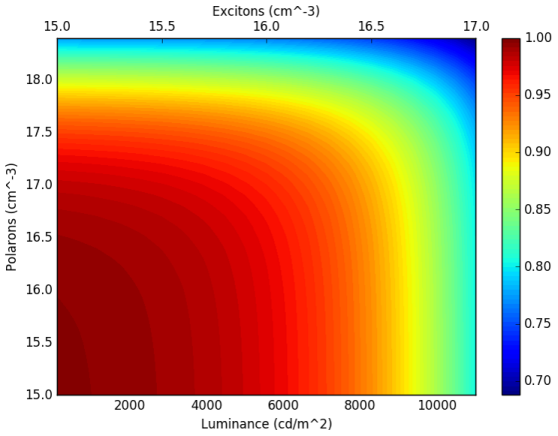

Figure 4.2: Multiplicative correction factor for exciton formation efficiency due to changes in quenching during lifetime. Shown as a function of polaron and exciton density as well as luminance, assuming a 10 nm emissive layer.

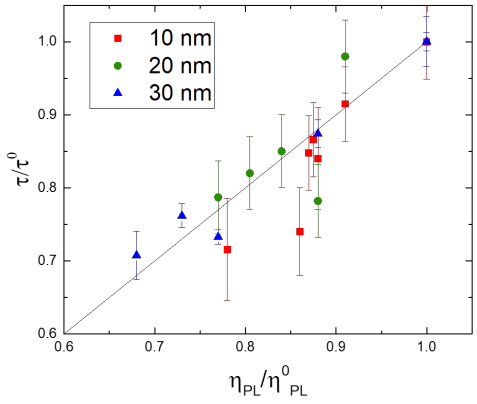

Figure 4.3: Exciton lifetime ratio extracted from transient PL measurements on degraded and undegraded devices as a function of emissive layer thickness.

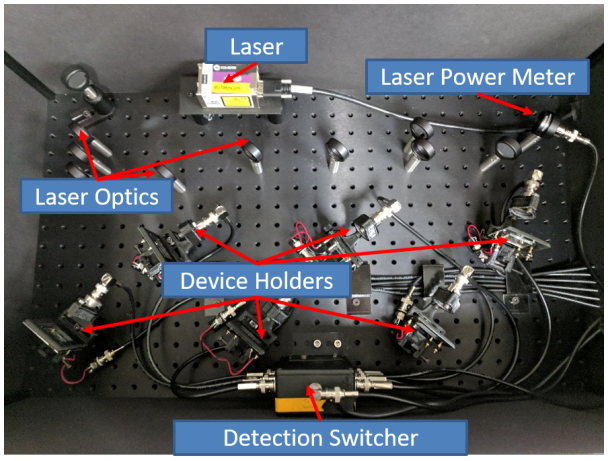

Figure 4.4: Device contacting, measurement, and optical hardware. Version 3 of the hardware is shown. Controlling hardware is shown in Fig. 4.5

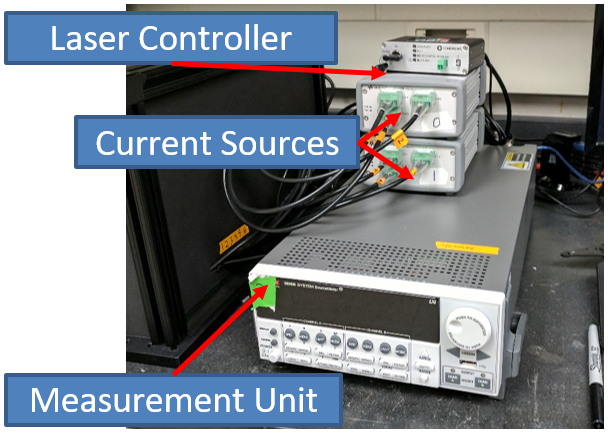

Figure 4.5: Source-Measure hardware and laser controller

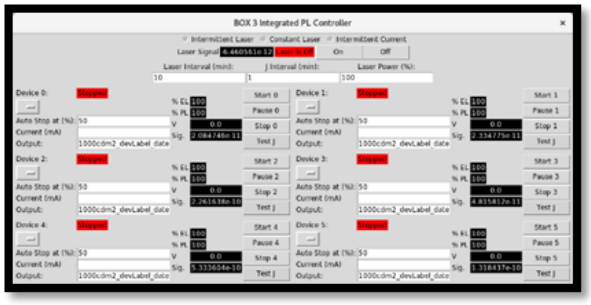

Figure 4.6: 6 channel software controller. Selection of test type, laser control for allignment, and global settings are accessible on the top of the interface. Individual channel settings are grouped on the bottom.

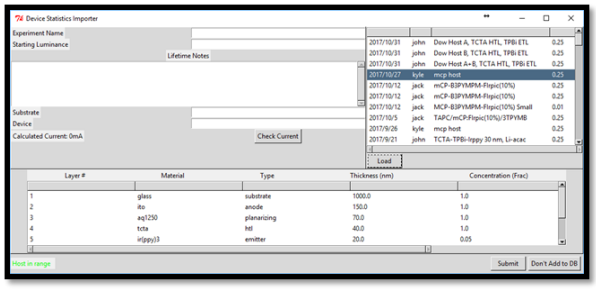

Figure 4.7: Test information for database import interface. The top left panel collects information about the specific device and lifetime. The right panel connects the device to a particular growth and architecture. The bottom panel confirms the architecture.

Chapter 5

Applied Integrated Lifetimes

5.1 CBP Host Thickness

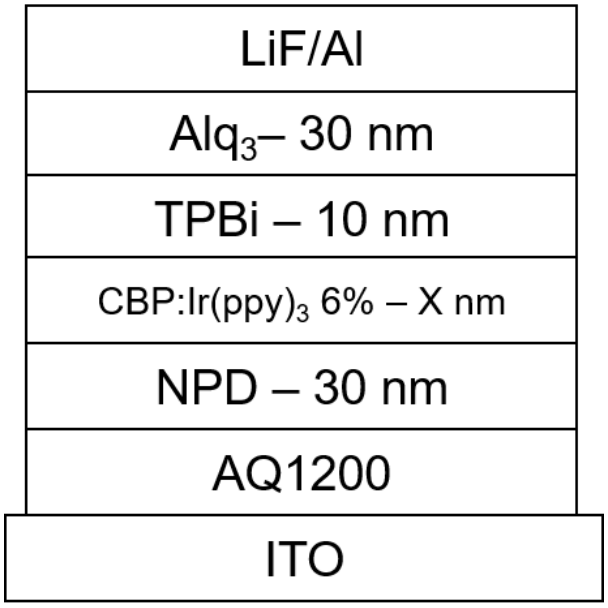

Figure 5.1: Device architecture, featuring EML thicknesses of X=10,20, and 30 nm

5.2 MEML Luminance Scaling

5.3 Dow Cohost

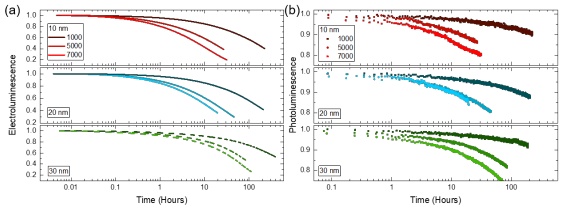

Figure 5.2: Device decay curves for multiple values of the initial luminance as a function of emissive layer thickness. Loss in (a) electroluminescence (EL) and (b) photoluminescence (PL) are shown and decrease monotonically with increasing luminance. For devices with a 10-nm-thick emissive layer, initial luminance values are 1000 cd/m^2, 5000 cd/m^2, and 7000 cd/m^2. For devices with a 20-nm- or 30-nm-thick emissive layer, initial luminance values are 1000 cd/m^2, 5000 cd/m^2, and 7100 cd/m^2.

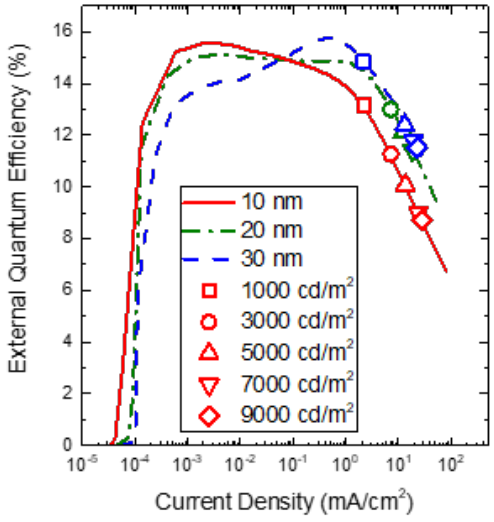

Figure 5.3: External Quantum Efficiency (η_{EQE}) for the three architectures. Operational points for lifetime are shown in symbols.

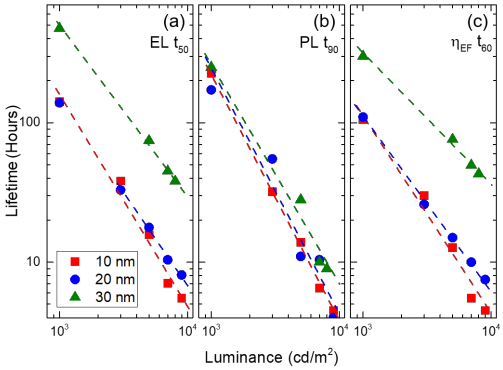

Figure 5.4: Extracted lifetimes for all 3 architecures as a function of luminance.

d_{EML} (nm)	L_0 (cd/m^2)	J (mA/cm^2)	V_0 (V)	t_{50} (hours)
10	1000	2.2	4.2	139.0
	3000	7.2	5.1	39.9
	5000	13.6	5.4	15.8
	7000	14.4	6.2	6.9
	9000	28.0	6.3	5.3
20	1000	2.2	5.4	141.1
	3000	7.2	6.0	33.1
	5000	12.4	7.2	17.2
	7100	19.2	7.3	10.0
	9000	24.0	7.5	8.0
30	1000	2.2	5.9	474
	5000	13.6	7.3	74.4
	7100	19.6	7.6	46
	8000	22.4	7.7	38.1

Table 5.1: Summary of device lifetimes. For each device, the starting luminance (L_0), current density (J), starting voltage (V_0) and time at which 50% of the initial luminance is reached (t_{50}) are reported.

Chapter 6

Novel Blue Emitter Developement

6.1 Molecular Systems

6.2 Performance Optimization

6.3 Solution Molecular Aggregation

Chapter 7

Data Management for Devices

Chapter 8

Modeling Out-Coupling

8.1 Theory

8.2 Recombination Zone Overlap During Lifetime

Chapter 9

Future Research

Bibliography

[1] Adachi, C., Kwong, R., and Forrest, S. R. Efficient electrophosphorescence using a doped ambipolar conductive molecular organic thin film. *Organic Electronics 2*, 1 (mar 2001), 37–43.

[2] Baldo, M., Adachi, C., and Forrest, S. R. Transient analysis of organic electrophosphorescence. II. Transient analysis of triplet-triplet annihilation. *Physical Review B 62*, 16 (oct 2000), 10967–10977.

[3] Baldo, M., O'Brien, D., You, Y., Shoustikov, A., Sibley, S., Thompson, M. E., and Forrest, S. R. Highly efficient phosphorescent emission from organic electroluminescent devices. *Nature 395*, September (1998), 151–154.

[4] Baldo, M., Thompson, M. E., and Forrest, S. High-efficiency fluorescent organic light-emitting devices using a phosphorescent sensitizer. *Nature 403*, 6771 (feb 2000), 750–3.

[5] Blom, P. W. M., De Jong, M. J. M., and Vleggaar, J. J. M. Electron and hole transport in poly(p-phenylene vinylene) devices. *Applied Physics Letters 68*, 23 (1996), 3308–3310.

[6] Erickson, N. C., and Holmes, R. J. Engineering efficiency roll-off in organic light-emitting devices. *Advanced Functional Materials 24* (2014), 6074–6080.

[7] Giebink, N. C., D'Andrade, B. W., Weaver, M. S., Brown, J. J., and Forrest, S. R. Direct evidence for degradation of polaron excited states in organic light emitting diodes. *Journal of Applied Physics 105*, 12 (2009), 124514.

[8] Giebink, N. C., and Forrest, S. R. Quantum efficiency roll-off at high brightness in fluorescent and phosphorescent organic light emitting diodes. *Physical Review B 77*, 23 (jun 2008), 235215.

[9] Hassine, L., Bouchriha, H., Roussel, J., and Fave, J. L. Transient response of a bilayer organic electroluminescent diode: Experimental and theoretical study of electroluminescence onset. *Applied Physics Letters 78*, 8 (2001), 1053–1055.

[10] Hassine, L., Bouchriha, H., Roussel, J., and Fave, J. L. Transient response of a bilayer organic light emitting diode: Building-up of external and recombination currents. *Journal of Applied Physics 91*, 8 (2002), 5170–5175.

[11] Hershey, K. W., and Cottingham, J. P. Material properties of pipes and reeds from the Southeast Asian khaen. *The Journal of the Acoustical Society of America 129*, 4 (apr 2011), 2520–2520.

[12] Hershey, K. W., and Holmes, R. J. Unified analysis of transient and steady-state electrophosphorescence using exciton and polaron dynamics modeling. *Journal of Applied Physics 120*, 19 (2016), 195501.

[13] Hershey, K. W., Suddard-Bangsund, J., Qian, G., and Holmes, R. J. Decoupling degradation in exciton formation and recombination during lifetime testing of organic light-emitting devices. *Applied Physics Letters 111*, 11 (2017), 113301.

[14] Holmes, R. J., Forrest, S. R., Tung, Y.-J., Kwong, R. C., Brown, J. J., Garon, S., and Thompson, M. E. Blue organic electrophosphorescence using exothermic hostguest energy transfer. *Applied Physics Letters 82*, 15 (2003), 2422.

[15] Kalinowski, J., Stampor, W., Mżyk, J., Cocchi, M., Virgili, D., Fattori, V., and Di Marco, P. Quenching effects in organic electrophosphorescence. *Physical Review B 66*, 23 (dec 2002), 235321.

[16] Kawamura, Y., Brooks, J., Brown, J. J., Sasabe, H., and Adachi, C. Intermolecular interaction and a concentration-Quenching mechanism of phosphorescent Ir(III) complexes in a solid film. *Physical Review Letters 96*, 1 (2006), 11–14.

[17] Kawamura, Y., Goushi, K., Brooks, J., Brown, J. J., Sasabe, H., and Adachi, C. 100% phosphorescence quantum efficiency of Ir (III) complexes in organic semiconductor films. *Applied Physics Letters 86*, 7 (2005), 1–3.

[18] Lampert, M. A. Volume-controlled current injection in insulators. *Reports on Progress in Physics 27*, 1 (2002), 329–367.

[19] Mezyk, J., Kalinowski, J., Meinardi, F., and Tubino, R. Triplet exciton interactions in solid films of an electrophosphorescent Pt (II) porphyrin. *Applied Physics Letters 86*, 11 (2005), 111916.

[20] Murawski, C., Leo, K., and Gather, M. C. Efficiency roll-off in organic light-emitting diodes. *Advanced materials (Deerfield Beach, Fla.) 25*, 47 (dec 2013), 6801–27.

[21] O'Brien, D. F., Baldo, M., Thompson, M. E., and Forrest, S. R. Improved energy transfer in electrophosphorescent devices. *Applied Physics Letters 74*, 3 (1999), 442.

[22] Pinner, D. J., Friend, R. H., and Tessler, N. Transient electroluminescence of polymer light emitting diodes using electrical pulses. *Journal of Applied Physics 86*, 9 (1999), 5116–5130.

[23] Pope, M., and Swenberg, C. *Electronic Processes in Organic Crystals and Polymers*, 2nd ed. Oxford University Press, 1999.

[24] Reineke, S., Schwartz, G., Walzer, K., Falke, M., and Leo, K. Highly phosphorescent organic mixed films: The effect of aggregation on triplet-triplet annihilation. *Applied Physics Letters 94*, 16 (2009), 2007–2010.

[25] Reineke, S., Schwartz, G., Walzer, K., and Leo, K. Reduced efficiency roll-off in phosphorescent organic light emitting diodes by suppression of triplet-triplet annihilation. *Applied Physics Letters 91*, 12 (2007), 1–4.

[26] Reineke, S., Walzer, K., and Leo, K. Triplet-exciton quenching in organic phosphorescent light-emitting diodes with Ir-based emitters. *Physical Review B 75*, 12 (mar 2007), 125328.

[27] Rihani, A., Hassine, L., Fave, J.-L., and Bouchriha, H. Study of the transient EL slow rise in single layer OLEDs. *Organic Electronics 7*, 1 (feb 2006), 1–7.

[28] Rothberg, L. J., and Lovinger, A. J. Status of and prospects for organic electroluminescence. *Journal of Materials Research 11*, 12 (1996), 3174–3187.

[29] Ruhstaller, B., Beierlein, T., Riel, H., Karg, S., Scott, J., and Riess, W. Simulating electronic and optical processes in multilayer organic light-emitting devices. *IEEE Journal of Selected Topics in Quantum Electronics 9*, 3 (2003), 723–731.

[30] Ruhstaller, B., Carter, S. a., Barth, S., Riel, H., Riess, W., and Scott, J. C. Transient and steady-state behavior of space charges in multilayer organic light-emitting diodes. *Journal of Applied Physics 89*, 8 (2001), 4575–4586.

[31] Song, D., Zhao, S., and Aziz, H. Modification of exciton lifetime by the metal cathode in phosphorescent OLEDs, and implications on device efficiency and efficiency roll-off behavior. *Advanced Functional Materials 21* (2011), 2311–2317.

[32] Song, D., Zhao, S., Luo, Y., and Aziz, H. Causes of efficiency roll-off in phosphorescent organic light emitting devices: Triplet-triplet annihilation versus triplet-polaron quenching. *Applied Physics Letters 97*, 24 (2010), 243304.

[33] Staroske, W., Pfeiffer, M., Leo, K., and Hoffmann, M. Single-Step Triplet-Triplet Annihilation: An Intrinsic Limit for the High Brightness Efficiency of Phosphorescent Organic Light Emitting Diodes. *Physical Review Letters 98*, 19 (2007), 197402.

[34] Tsuboi, T., Murayama, H., and Penzkofer, A. Photoluminescence characteristics of Ir(ppy)3 and PtOEP doped in TPD host material. *Thin Solid Films 499*, 1-2 (2006), 306–312.

[35] Tsutsui, T., Yang, M.-j., Yahiro, M., Nakamura, K., Watanabe, T., Tsuji, T., Fukuda, Y., Wakimoto, T., and Miyaguti, S. High Quantum Efficiency in Organic Light-Emitting Devices with Iridium-Complex as a Triplet Emissive Center. *Jpn. J. Appl. Phys. Part 2: 38*, 12 (1999), L1502–L1504.

[36] Turro, N., Scaiano, J., and Ramamurthy, V. *Modern Molecular Photochemistry of Organic Molecules*. University Science Books, 1991.

[37] Wei, B., Furukawa, K., Amagai, J., Ichikawa, M., Koyama, T., and Taniguchi, Y. A dynamic model for injection and transport of charge carriers in pulsed organic light-emitting diodes. *Semiconductor Science and Technology 19*, 5 (may 2004), L56–L59.

[38] Xu, F., Hershey, K. W., Holmes, R. J., and Hoye, T. R. Blue-Emitting Arylalkynyl Naphthalene Derivatives via a Hexadehydro-Diels?Alder Cascade Reaction. *Journal of the American Chemical Society 138*, 39 (oct 2016), 12739–12742.

[39] Zhang, B., Tan, G., Lam, C. S., Yao, B., Ho, C. L., Liu, L., Xie, Z., Wong, W. Y., Ding, J., and Wang, L. High-efficiency single emissive layer white organic light-emitting diodes based on solution-processed dendritic host and new orange-emitting iridium complex. *Advanced Materials 24*, 14 (2012), 1873–1877.

Appendices

Appendix A

List of Publications

- Hershey, K. W., and Cottingham, J. P. Material properties of pipes and reeds from the Southeast Asian khaen. *The Journal of the Acoustical Society of America 129*, 4 (apr 2011), 2520–2520
- Hershey, K. W., and Holmes, R. J. Unified analysis of transient and steady-state electrophosphorescence using exciton and polaron dynamics modeling. *Journal of Applied Physics 120*, 19 (2016), 195501
- Hershey, K. W., Suddard-Bangsund, J., Qian, G., and Holmes, R. J. Decoupling degradation in exciton formation and recombination during lifetime testing of organic light-emitting devices. *Applied Physics Letters 111*, 11 (2017), 113301
- Xu, F., Hershey, K. W., Holmes, R. J., and Hoye, T. R. Blue-Emitting Arylalkynyl Naphthalene Derivatives via a Hexadehydro-Diels?Alder Cascade Reaction. *Journal of the American Chemical Society 138*, 39 (oct 2016), 12739–12742

A.1 Measuring Triplet Energies

A.2 Single Carrier Device Modeling

Appendix B

Out-Coupling Code

Appendix C

Lifetime Box Code

List of Figures

List of Tables